DOI: 10.1002/ejic.200700990

Versatility of Laser Pyrolysis Applied to the Synthesis of TiO_2 Nanoparticles – Application to UV Attenuation

Bruno Pignon,[a] Hicham Maskrot,[a,b] Véronique Guyot Ferreol,[c] Yann Leconte,[a] Servane Coste,[a,d] Monique Gervais,[b] Thierry Pouget,[c] Cécile Reynaud,[a] Jean-François Tranchant,[c] and Nathalie Herlin-Boime*[a]

Keywords: Laser pyrolysis / TiO_2 / TiON / Nanoparticles / Nanocrystals

TiO_2 nanoparticles show interesting catalytic and optical properties and are therefore highly demanded for several applications. In this paper, we show that pure and N-doped TiO_2 powders with an average diameter as low as 8 nm can be synthesized by laser pyrolysis, with the use of an aerosol of TTIP (titanium tetraisopropoxide) as the main precursor sensitized by C_2H_4. We demonstrate the possibility to control the anatase/rutile phase ratio over a large range, which was not achieved before, by tuning the experimental parameters. N-doped particles have also been produced for the first time by this method by using a one-step process through addition of NH_3. First results illustrating the consequences in terms of UV absorption properties are also presented and correlated with the structural evolution and the presence of a doping element.

Introduction

Owing to a large field of applications (paint pigments, cosmetics, catalysis, and photocatalysis), many studies have been devoted to titania nanoparticles. Some of the interesting properties of TiO_2 strongly depend on the crystalline phase, and the incorporation of heteroatoms can enhance photocatalytic activity as well as the absorption of solar light. In this context, it is particularly interesting to be able to synthesize such nanoparticles with, on the one hand, an accurate control of the crystalline phase ratio, and, on the other hand, the possibility to add different doping elements to titania.

These titania nanoparticles are obtained by various chemical or physical methods. Among the wet chemical methods, sol–gel synthesis with titanium tetraisopropoxide (TTIP) as precursor has been widely developed. This method allows producing crystallized nanoparticles mainly in anatase form. Further treatments are then required to achieve crystallization in the rutile phase (see, for example, refs.[1,2]). As for the incorporation of heteroatoms, colloidal chemistry has been used to obtain TiO_xN_y nanoparticles by means of annealing under an NH_3 atmosphere.[3,4] The main limitation of this chemical method is the batch production of nanoparticles.

Gas-phase synthesis methods can be useful for achieving a continuous production of nanoparticles. Among the gas-phase methods, flame synthesis is an efficient way of producing TiO_2 nanocrystals (see, for example, ref.[5]) by using TTIP or $TiCl_4$ as precursors. Without addition of metals such as Al, titania was obtained mainly in the anatase phase. Another gas-phase method is pyrolysis by a CO_2 laser. Its versatility has already been demonstrated for the synthesis of silicon-based nanoparticles.[6] Since 1987, this technique has also been used to synthesize TiO_2 nanoparticles from various titanium alkoxides such as TTIP,[7,8] titanium butoxide,[7] titanium ethoxide,[9] or from titanium chloride.[10] In most cases, the main crystalline phase was once again anatase. Nevertheless, the latest developments in laser pyrolysis open up new possibilities in terms of controlling particle-growth mechanisms, i.e. the possibility to tune the reaction parameters (duration, temperature) in order to control the final structure and composition (grain size, crystalline phase, stoichiometry) of the nanoparticles produced, and, as a consequence, their properties.

In this paper, we show that it is possible to produce TiO_2 nanocrystals in large amounts by laser pyrolysis of liquid TTIP, which is a safer precursor than $TiCl_4$. We demonstrate that changing various synthesis parameters enables the efficient control of the anatase/rutile ratio over a very large range, which was not achieved before. In the second part of this paper, we report for the first time the synthesis

[a] Service des Photons, Atomes et Molécules, Laboratoire Francis Perrin (CEA-CNRS URA 2453), CEA Saclay, 91191 Gif/Yvette Cedex, France
E-mail: nathalie.herlin@cea.fr
[b] Laboratoire d'électrodynamique des Matériaux Avancés (UMR CEA-CNRS 6157), Université François Rabelais, Parc de Grandmont 37200 Tours, France
[c] LVMH Recherche, Parfums & Cosmétiques, Département Innovation Matériaux et Technologies, Saint Jean de Braye, France
[d] Unité d'Enseignement Science de la Matière et Simulation/INSTN-CEA Saclay, 91191 Gif sur Yvette Cedex, France

of TiO_xN_y nanoparticles by laser pyrolysis by addition of NH_3 in the reaction zone. Moreover, these N-doped nanoparticles are obtained in a one-step process. Finally, the optical properties of such titania-based nanoparticles are expected to be very sensitive to the structure, and UV range absorption measurements of the particles are also addressed and correlated with the evolution of the bandgap of the different crystalline forms of titania.

Results and Discussion

Synthesis and Optical Properties of TiO_2 Nanoparticles

Table 1 summarizes the different experimental conditions used to synthesize the five different TiO_2 samples presented in this work, together with their as-synthesized content in free C calculated from TGA measurements. This evolution of the carbon content is also evident from the color change in the as-formed powders; the color changes from almost white (sample A with low carbon content) to dark gray (sample E with the highest carbon content). Samples A and B only differ in the kind of carrier gas (CG) used. During the syntheses, the differences in the pyrolysis flame could be seen with the naked eye: for sample A the flame intensity was low because of the cooling effect of He. As a result of this lower flame temperature, TTIP and C_2H_4 decompose to a lower extent, and thus sample A has a lower free C content than sample B. It is also important to note that the reaction was better confined with Ar as CG than with He.

Table 1. Synthesis parameters and as-formed C content.

Sample	C_2H_4 flow rate [slm]	CG	Laser power [W]	C [wt.-%]
A	1.6	He	650	3.0
B	1.6	Ar	650	4.2
C	1.6	Ar	750	7.2
D	1.6	Ar	850	9.4
E	0.8	Ar	2100	18.2

Samples B to D differ by the laser power which was progressively increased from 650 to 850 W. The higher the laser power, the brighter the flame appeared during the synthesis. This observation gives evidence of the predictable reaction temperature increase with the laser power. As a consequence, the decomposition of the different C precursors was enhanced, which led to a larger amount of free C in the final powder.

For sample E, the laser power was increased up to 2100 W. The reaction temperature, and thus C production, was so high that the C_2H_4 sensitizer gas (SG) flow had to be decreased down to 0.8 slm in order to obtain reasonable contents of free C in the final product.

As the free C content is not a matter of interest for the application aimed in this study, the samples were annealed in order to remove this byproduct (see Experimental Section for annealing details). The effect of such treatment will be checked in the following discussion.

The crystalline nature of the samples was first investigated by means of XRD measurements. The effect of reaction temperature was examined by comparison of the samples A and E representative for low- and high-temperature synthesis conditions, respectively. Recorded patterns are presented in Figure 1, before (as formed) and after annealing (annealed), together with references for the anatase (JCPDS file 21-1272) and rutile (JCPDS file 21-1276) phases. Looking at the as-formed powders first, we can see that both samples consist mainly of a mixture of rutile and anatase phases. It can already be noticed that the "high-temperature" sample E appears to be much richer in the rutile phase than the "low-temperature" sample A, but we will come back to this point later. From the annealing effect point of view, no major change in terms of crystalline phase ratio or peak width can be observed on the diagrams. Thus, the structure and size of the nanocrystallites do not seem to be strongly affected by the soft heat treatment used to remove free C. In the following, all the presented results are focussed on annealed samples.

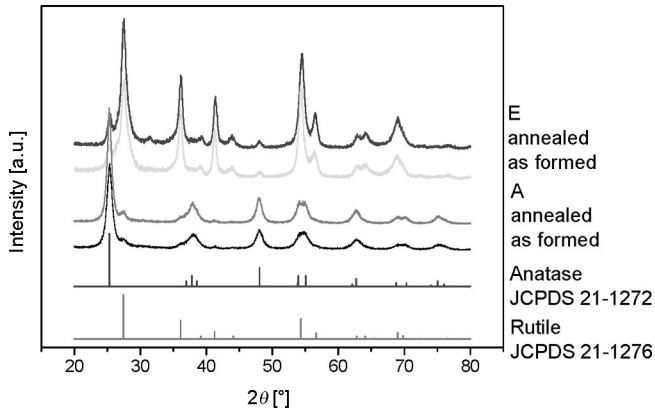

Figure 1. XRD patterns recorded with as-formed and annealed samples synthesized at low temperature (sample A) and high temperature (sample E).

Figure 2 presents the XRD patterns recorded for all the samples after annealing compared to references for the pure anatase and rutile phases.

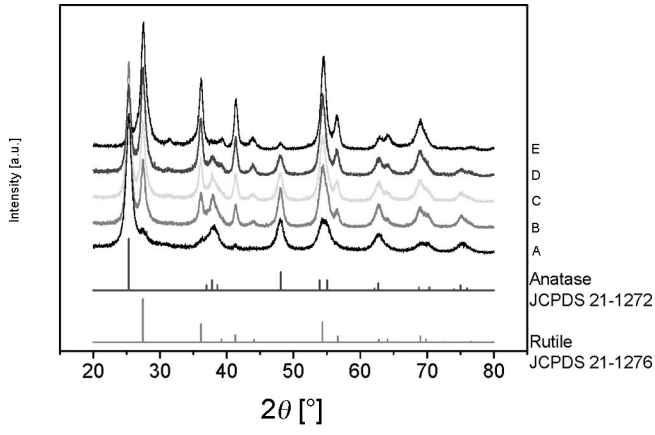

Figure 2. XRD patterns recorded with annealed samples (see Table 1) with anatase and rutile peak positions.

As mentioned previously, all the powders consist of mixtures of the anatase and rutile phases. To evaluate the anatase/rutile ratio, a quantification of these phases was performed by the Rietveld quantification method. The results are summarized in Table 2 together with measurements of diameter and *A*.

Table 2. Characterization results for annealed TiO_2 samples.

Annealed sample	Anatase [wt.-%]	Rutile [wt.-%]	BET diameter [nm]	TEM diameter [nm]	UV absorption coefficient, *A*
A	85	15	13.8.	8	95
B	60	40	14.4	13	191
C	47	53	13.6	10	229
D	32	68	14.4	10	339
E	10	90	23.0	21	529

The anatase content ranges from 85 to 10 wt.-% correlated with the synthesis conditions. From the structural point of view, rutile is known to be the TiO_2 high-temperature phase and anatase the low-temperature one; it is therefore logical to favor the high temperature phase with increasing the flame temperature as in the case of sample E. To the best of our knowledge, such a control of the phase ratio over a wide range of percentages has never been achieved by a gas-phase method for nanoparticle synthesis. Controlling the rutile content is very important, as some properties of titania, especially UV absorption, are strongly dependent on the crystalline phase.

The powders were also characterized by BET and TEM in order to determine the grain size of the samples. The BET diameter was calculated by using the measured value of 4.0 for the relative density. The relative density of the annealed powder was measured by pycnometry and was in good agreement with that of a mixture of anatase (theoretical relative density: 3.9) and rutile (theoretical relative density: 4.2). The results are reported in Table 2. The corresponding TEM pictures for samples A, C, and E are presented in Figure 3 together with bar graphs presenting the size distribution. These graphs were obtained by counting the number of particles of a given diameter in a total number of 200 nanoparticles. The TEM diameter given in Table 2 is an average calculated from the values in these bar graphs. In general, it can be noted that the sizes calculated from BET measurements are slightly larger than the ones obtained from TEM observations. This can be related to the agglomeration of the powders.

The TEM pictures presented in Figure 3 show the general morphology of the nanoparticles: they are most often roughly spherically shaped even if some of them appear to be facetted. The particles are arranged in a chain-like manner, and usually most of the weak electrostatic bonds connecting the particles can easily be broken in solution by ultrasound dispersion treatment as shown by PCS (Photon Correlation Spectroscopy) measurements. The reported size distributions appear to be relatively narrow.

From the size evolution point of view, only the sample synthesized at the highest laser power (E) shows significantly larger grains when compared to all other samples. This observation is certainly a temperature effect. Indeed, in laser pyrolysis, as in other gas-phase methods, it is well known that the growth and coalescence of the particles are enhanced by an increase in the temperature

If we now turn to the evolution of the optical properties, Figure 4 allows a comparison of the five samples, with different contents in rutile and anatase as described previously, by plotting their UV transmittance. In case of sample A, the anatase/rutile ratio is 85:15 and it changes to 10:90 in the case of sample E (see Table 2). In the 340–400 nm range, a strong modification of transmitted UV light intensity can be observed: the higher the rutile content, the weaker the transmitted light intensity and the more efficient the filtration of UV. For samples B, C, and D, it is important to remark that the differences in UV absorption can only be

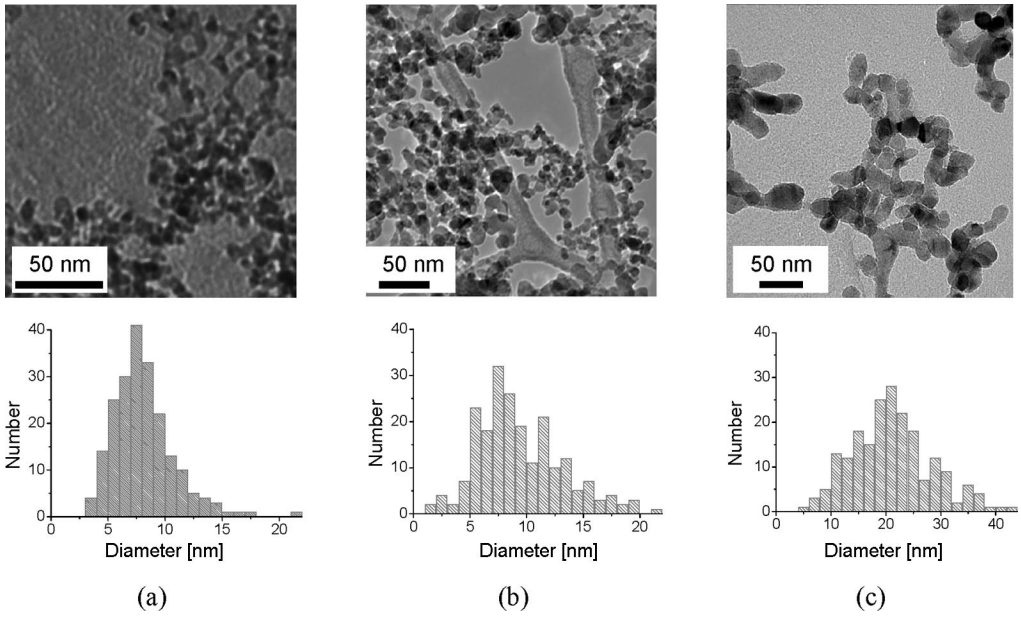

Figure 3. TEM pictures and size distributions for samples A (a), C (b), and E (c).

ascribed to the phase ratio, as the grain sizes are very similar (see Table 2). Therefore, the improvement in UV filtration can be correlated to the percentage of the rutile phase as expected from the well-known difference in the optical properties of the rutile and anatase phases, the former one being more efficient than the latter one in UV absorption. In fact, the efficiency in terms of transmission in this spectral range is related to the electronic properties of the solids. The position of the anatase bandgap is 384 nm while it is 411 nm for TiO_2 in the rutile phase. In good agreement with these bandgap positions, Figure 4 clearly shows that the TiO_2 coating begins to transmit the light at larger wavelengths when the rutile content in the powder increases.

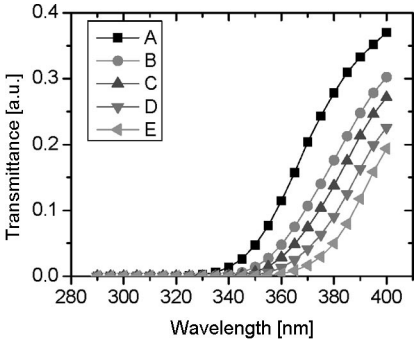

Figure 4. UV transmission of samples A to E. (increasing rutile content from A to E).

From the data of transmitted light intensity presented in Figure 4, the attenuation coefficient A (values also reported in Table 2) was calculated by using an algorithm described by Diffey.[11] The obtained values were plotted as a function of the rutile content; the corresponding graph is shown in Figure 5.

The influence of the rutile content can also be observed on this curve, independently of size effects. There is clearly a good correlation between the properties of attenuation in the UV range and structural order and it is possible to quantify this effect. This demonstrates the ability of laser pyrolysis to control the UV transmission properties of the nanoparticles.

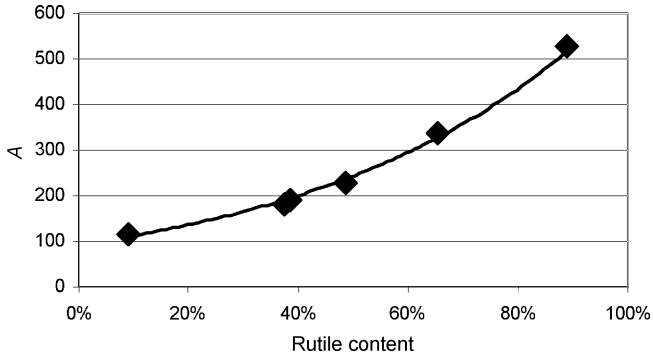

Figure 5. Evolution of the attenuation coefficient, A, as a function of rutile content [wt.-%] (the line is just a guide for the eyes).

Synthesis and Optical Properties of TiO_xN_y Nanoparticles

The N-doped samples studied here were obtained with the same synthesis parameters as those for the TiO_2 sample A, which was compared to the other samples in terms of the parameters laser power and CG in the previous discussion. A flow of NH_3 (400 sccm) was added to He as CG in order to introduce nitrogen into the reaction. The obtained powder is shown in Figure 6 before (a) and after (b) annealing. It can clearly be seen that the thermal treatment makes the powders turn from green to yellow.

The yellow color, which has already been observed in such compounds, see ref.[3] for example, is attributed to the presence of nitrogen atoms, which was confirmed by infrared spectroscopy and XPS data (not presented here). The N content in this powder was measured to be 0.9 atom-% by chemical analysis (CNRS, Vernaison). The green color is attributed to a mixture of yellow (presence of nitrogen) and blue coming from nonstoichiometric titania $TiO_{2-\varepsilon}$ which has already been observed in titanium-based compounds obtained from laser pyrolysis.[12] This substoichiometry of titania is due to a partial reduction of the oxide during the synthesis in the reductive atmosphere obtained with NH_3. After annealing in air, the stoichiometry of oxygen is recovered, and the blue color disappears, leaving only the yellow color of nitrogen-rich titania. Note that the car-

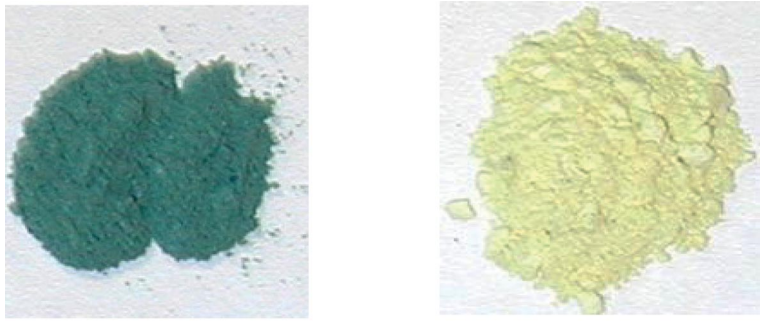

Figure 6. Macroscopic aspects of the as-formed (a) and annealed powders (b).

bon content in this sample was low in the as-formed powder (3 atom-%).

Figure 7 presents the XRD diagram of the as-formed N-doped sample, which exhibits only the peaks of anatase phase, with no trace of rutile, in contrast to the previous set of experiments.

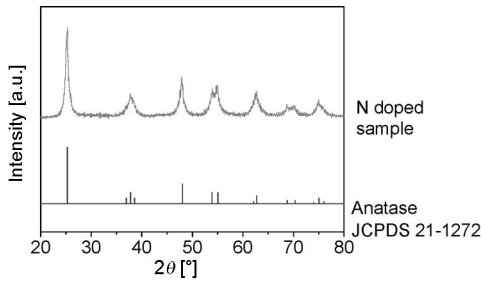

Figure 7. XRD patterns recorded with the as-formed N-doped sample with anatase peak positions.

Figure 8 presents the morphology of the sample observed by TEM together with the corresponding size distributions of the as-formed (a) and annealed (b) samples. The average size and size distributions obtained by counting 200 nanoparticles do not indicate significant morphological changes after the annealing. The size calculated from BET (19 and 21 nm for as-formed and annealed powders, respectively) is larger than the one evaluated from TEM (9 and 10 nm for as-formed and annealed powders, respectively) measurements, indicating a higher degree of agglomeration in the powder relative to the TiO_2 samples.

Figure 9 presents the transmittance curve obtained for the annealed N-doped sample, together with the curves recorded for the pure TiO_2 samples A and E presented in the previous section. For the N-rich sample, the maximum transmitted intensity is only 0.07, which is lower than the values recorded for all other pure TiO_2 samples. It corresponds to A = 700, the best value obtained for this set of samples. It must be noted that in this sample exhibiting the best UV attenuation, only the anatase crystalline form was identified. The presence of doping nitrogen atoms in the TiO_2 network contributes to bandgap narrowing. Therefore a redshift of the absorption edge to a longer wavelength, as compared to titania, is observed in the N-doped samples.[3,4] This shift corresponds to a lower transmission in the 290–400 nm range and to an efficient UV absorption. Finally, the TiO_xN_y sample absorbs even better than the rutile-rich pure TiO_2 sample.

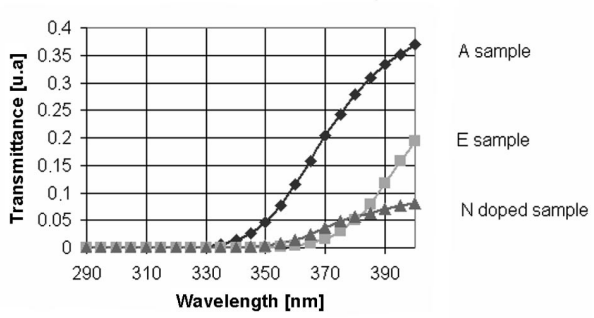

Figure 9. UV transmission of annealed N-doped sample (triangle) together with pure TiO_2 samples A (diamond) and E (square).

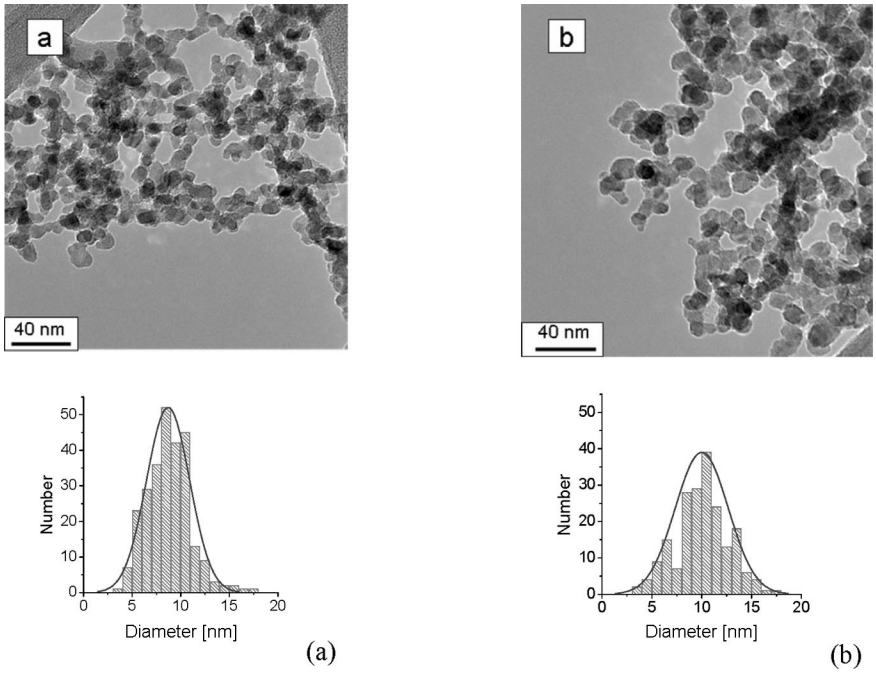

Figure 8. (a) TEM pictures and size distribution of the as-formed N-doped sample; (b) TEM pictures and size distribution of the annealed N-doped sample.

Conclusion

This study has shown for the first time that, with the laser pyrolysis technique, the control of the reaction temperature allows controlling the crystalline phase of TiO_2 nanocrystals. Depending on experimental conditions, TiO_2 nanocrystals are obtained in the 8–20-nm diameter range, and the ratio of the crystalline phases varies over a large range from mainly anatase to mainly rutile. Moreover, we have shown that laser pyrolysis allows easy synthesis of N-doped nanocrystals. The change in structural organization (rutile to anatase ratio) and in electronic structure (N-doped or pure TiO_2) has been correlated with the evolution of UV absorption properties. An increase in the rutile content or the introduction of nitrogen atoms into the TiO_2 network improves the UV absorption properties. Further measurements will involve, on the one hand, the determination of the optical gap and measurement of the absolute absorption coefficient as a function of rutile content in the powder, and, on the other hand, the better investigation of the electronic structure of the N-doped samples.

Experimental Section

The laser pyrolysis technique is based on the resonance between the emission of a CO_2 laser (10.6 μm) and the absorption of a gaseous or liquid precursor.[9] The experimental setup with aerosol generator, reaction chamber, and powder collector has already been described.[13] The confinement of the precursor flow by an argon or helium chimney right at the exit of the inlet nozzle avoids any reaction with the reactor walls, protecting the powders from any contamination. The main synthesis parameters are pressure, laser power, composition of the reactant mixture, and flow rate of the precursor stream. All these parameters play a key role in determining the reaction temperature and reaction time, which are responsible for the final grain size and structure of the powder. When compared to other nanoparticle synthesis techniques, the size distribution appears to be very narrow.

For TiO_2 synthesis, liquid TTIP was supplied by Sigma–Aldrich and used without further purification. The TTIP aerosol was produced by an ultrasonic spraying technique (Pyrosol process) and carried to the reaction chamber by a carrier gas (CG) flow through a nozzle 6 mm in diameter. The CG also acts as a diluent for the reagents, so in addition to the TTIP feeding rate control, the properties of the CG can also influence the reaction temperature. In this context, He was compared to Ar because of its higher specific heat. CG flow was fixed to 2 slm, leading to a TTIP feeding rate of 25 $g\,h^{-1}$ with He and 40 $g\,h^{-1}$ with Ar. Since TTIP poorly absorbs the laser radiation, a sensitizer gas (SG), C_2H_4, was also added. C_2H_4 and TTIP aerosol were mixed just before the exit of the inlet nozzle so that C_2H_4 would not participate in the aerosol carrying. The flow of reactants intersects the laser beam orthogonally. The reactor pressure was fixed to 740 Torr, and the laser power was varied in the 650–2100 W range.

For TiO_xN_y synthesis, NH_3 (400 sccm) was added to the CG in order to provide N atoms. As this gas absorbs the laser radiation, no addition of SG was needed for these experiments.

After the synthesis, the obtained powders contained free C atoms coming from TTIP and/or C_2H_4 decomposition. In order to remove these C atoms, the samples were submitted to soft thermal treatment in air. Annealing treatments were carried out in a Nabetherm HTO8/1750 furnace. Samples were heated up to 400 °C at 5 °C min^{-1}, kept at this temperature for 3 h and cooled down to room temperature at 20 °C min^{-1}. These annealing conditions were determined by previous thermogravimetric analyses (TGA) in order to ensure the complete removal of free C. These latter measurements have also led to the accurate determination of the C content in the as-formed powders.

The specific surface areas (S_{BET}) were measured by the BET (Brunauer–Emmet–Teller) method with a Micromeretics Flowsorb 2300. Assuming a round shape for the nanoparticles, the diameter, D, was calculated from the surface measurement (S_{BET}) by using the formula $D = 6/(\rho S_{BET})$, where ρ is the density. The morphology was studied by transmission electron microscopy (TEM) with a Philips CM12 (120 kV) instrument. X-ray diffraction (XRD) patterns were obtained at room temperature by using a Bragg Brentano diffractometer (Siemens D5000) in θ–2θ geometry with a Cu anticathode (Cu-K-L_2, Cu-K-L_3, λ = 1.540598 and 1.544390 Å) and a secondary monochromator. The 20–80° (2θ) angular range was scanned in 0.02° (2θ) steps with a counting time set at 10 s $step^{-1}$. Rietveld refinements were performed with the Fullprof 2000 program for phase quantification.[14] Thermogravimetric analysis was performed with a 92–16.18 Setaram instrument. Samples were analyzed in an alumina crucible at a heating rate of 5 °C min^{-1} to 1000 °C in an atmosphere of air flowing at 50 mL min^{-1}.

In order to address the optical properties of the obtained nanopowders, the following sample preparation was applied: in a first step, the powders were disagglomerated by means of a grinder with plates (J. Engelsmann AG type JEL 25/53) by adding some castor oil to a binder. The ratio of nanopowder to castor oil was 0.5:2. In a second step, the mixture was scattered under ultrasound in a collodion composed of nitrocellulose (15%) and a 50:50 mixture of ethyl and butyl acetate (85%). Finally, the nanopowder dispersion was deposited on PMMA plates with an automatic film applicator (PIAB type Lab Vac LVX20) and a mobile having a step of 300 μm. After the film dried, measurements of transmitted light intensity were performed between 290 and 400 nm with a Scientec OL 754 spectrophotometer with a 75 W xenon arc lamp in order to have an incident light composition close to that of solar light. The absorption curves are plotted by measuring the transmitted intensity of the sample (powder + nitrocellulose + oil + PMMA) compared to a reference sample (nitrocellulose + oil + PMMA). These transmission measurements allow the calculation of an UV attenuation coefficient (A) with the procedure described by Diffey.[11]

Acknowledgments

This work was granted by a national performance program, NAMICERCOS (NAnostructures MInérales pour la CERamique et la COSmétique). The authors would like to thank their colleague B. Bouchet-Fabre for XPS spectroscopy and fruitful discussions.

[1] J. Livage, M. Henry, C. Sanchez, *Prog. Solid State Chem.* **1988**, *18*, 259–341.
[2] S. Doeuff, Y. Dromzee, F. Taulelle, *Inorg. Chem.* **1989**, *28*,. 4439–4445.
[3] C. Burda, Y. Lou, X. Chen, A. Samia, J. Stout, J. Gole, *Nano Lett.* **2003**, *3*, 1049–1051.
[4] R. Asahi, T. Morikawa, T. Ohwaki, K. Aoki, Y. Taga, *Science* **2001**, *293*, 269–271.
[5] S. E. Pratsinis, W. Zhu, S. Vemury, *Powder Technol.* **1996**, *86*, 87–93.

[6] W. R. Cannon, S. C. Danforth, J. H. Flint, J. S. Haggerty, R. A. Marra, *J. Am. Ceram. Soc.* **1982**, *65*, 330–335.
[7] J. D. Casey, J. S. Haggerty, *J. Mater. Sci.* **1987**, *22*, 4307–4312.
[8] M. Grujic-Brojcin, M. Scepanovic, Z. Dohcevic-Mitrovic, I. Hinic, B. Matovic, G. Stanisic, Z. Popovic, *J. Phys. D* **2005**, *38*, 1415–1420.
[9] F. Curcio, M. Musci, N. Notaro, G. De Michele, *Appl. Surf. Sci.* **1990**, *46*, 225–229.
[10] R. Alexandrescu, F. Dumitrache, I. Morjan, I. Sandu, M. Savoiu, I. Voicu, C. Fleaca, R. Piticescu, *Nanotechnology* **2004**, *15*, 537–545.
[11] B. L. Diffey, J. Robson, *J. Soc. Cosmet. Chem.* **1989**, *40*, 127–133.
[12] H. Maskrot, N. Herlin-Boime, Y. Leconte, K. Jursikova, C. Reynaud, J. Vicens, *J. Nano Res.* **2006**, *8*, 351–360.
[13] M. Cauchetier, O. Croix, N. Herlin, M. Luce, *J. Am. Ceram. Soc.* **1994**, *77*, 993–998.
[14] J. Rodriguez-Carvajal, FULLPROF version 2.60, March **2004**.
Received: September 16, 2007
Published Online: January 25, 2008

